Analysis of Limitations of SCCWRP Variant ROMS-BEC Model Source Code

Final: 31 October 2022; Revised: 4 January 2023

Submitted by:
Scott A. Jenkins, Ph.D. and Makrom Shatila, P.E.
Michael Baker International
9755 Clairmont Mesa Blvd
San Diego, CA 92124

Submitted to:
Amber Baylor, M.S., M.P.A., BCES
Director of Environmental Compliance
South Orange County Wastewater Authority
34156 Del Obispo St.
Dana Point, CA 92629

Notice to Reader:

This is a revision of the 31 October 2022 draft final that was prompted by receipt of additional information following a ROMS/BEC review meetings held at San Diego Regional Water Quality Control Board on 8 December 2022 and at SCCWRP headquarters in Costa Mesa, CA, on 12 December 2022.

1. Summary of Findings:

We find two (2) significant omissions in the model code of the Southern California Coastal Water Research Project (SCCWRP) variant of their Regional Ocean Modeling System (ROMS) / Biogeochemical Elemental Cycling (BEC) model, which bias its results toward over stimulation of plankton growth rates and under-prediction of outfall dilution rates, both of which provoke plankton blooms that ultimately contribute to ocean acidification and hypoxia (OAH) through the decay (RedOx) processes following bloom die off. These omissions are:

1) The SCCWRP variant of ROMS/BEC omits scattering physics in the formulation of light attenuation throughout the water column. In coastal waters, back scattering by tiny suspended particulate (particle sizes in the range of $0.1\ \mu\text{m} \le D \le 1\ \mu\text{m}$) accounts for 70% to 80% of total light attenuation, while absorption attenuates only the remaining 20% or 30% of the downwelling irradiance. Consequently, omission of back scattering in the formulation of available light leads to a deeper photic zone with higher light intensity at

any given depth, both of which result in higher photosynthetic rates and growth rates than would otherwise be predicted if back-scattering had been included.

2) The schematization of the dilution of effluent discharges from ocean outfalls is lacking in the SCCWRP variant of ROMS/BEC by assuming a fixed, time-invariant mixing volume which never occurs in Nature. The mixing volume of a prototypic scale outfall plume in Nature varies continuously over time in response to the vertical variations in temperature/salinity profiles, winds, waves, currents and outfall specific parameters such as discharge rates, diffuser length, numbers and size of discharge ports; none of which the assumed fixed, time invariant ROMS/BEC formulation of the mixing volume can replicate or even adequately approximate. Consequently, the SCCWRP variant of ROMS/BEC under-predicts the dilution that occurs in the modeled outfall plumes; which in turn, leads to higher undiluted nitrate and ammonia concentrations in the outfall plumes, thereby imparting a bias in favor of excessive plankton photosynthetic rates and growth rates stimulated by excessive nutrient concentrations of anthropogenic origins. In other words, this significant flaw leads directly toward implicating ocean outfalls as the cause of plankton blooms and OAH.

These omissions in the codes of the SCCWRP variant of ROMS/BEC model were presented to the San Diego Regional Water Quality Control Board on 8 December 2022, following the latest SCCWRP update on their validation efforts of the ROMS/BEC model. Because the SCCWRP variant of ROMS/BEC has omissions in its model codes that bias its results toward excessive plankton growth rates and under-prediction of outfall dilution rates, it is not yet sufficiently well-developed to be used as a tool to guide regulatory or legislative policy formulation. In its present undeveloped state, this model should not be required to assess OAH causality in the ocean environment around each individual outfall as a condition for the reissuance of NPDES permits for those outfalls.

2. Introduction:

ROMS/BEC is a multi-disciplinary process-based modeling system consisting of an ocean circulation model, the *Regional Oceanic Modeling System* (ROMS), coupled to a geochemical model that provides nutrients to an ichthyoplankton growth model, the *Biogeochemical Elemental Cycling* (BEC) model. At the outset, it should be recognized that many different variants of ROMS/BEC models have been developed over the past 3 decades; the first being developed by the US Navy in the 1990's to predict optical properties of the coastal ocean water mass in order to support imagery of underwater targets using multi-spectral scanners flown aboard air-born and space-born platforms (cf. Hammond, et al, 1995). A particular ROMS/BEC variant is being promoted by the Southern California Coastal Waters Research Program (SCCWRP), for the expressed purpose of using it as a tool to guide regulatory or legislative policy, (cf. "Management Scenarios" in Sutula, 2019). The need for such a tool is based on the SCCWRP hypothesis that anthropogenic sources of nutrients (principally municipal ocean outfalls) are causing *ocean acidification and hypoxia* (OAH) in the Southern California Bight (SCB). This OAH hypothesis is based on the notion that over-nutrification of the coastal ocean by discharges from municipal outfalls produce excessive growth rates in *plankton* populations,

commonly referred to as *algal blooms,* which eventually die off. The decay of the overly-abundant dead plankton, through reduction/oxidation reactions, or RedOx, depletes oxygen while converting the organic carbon of the dead organisms back into dissolved CO_2 which forms carbonic acid H_2CO_3 and disassociates into carbonate CO_3^{2-} or bicarbonate HCO_3^- ions and free hydrogen ions H^+, the latter causing acidification. Therefore, the underpinning of the SCCWRP hypothesis is tied to excessive growth rates of plankton populations which are limited by the availability of nutrients and light.

In order for the SCCWRP hypothesis to be considered well proven and suitable to guide regulatory or legislative policy formulation, an extraordinary degree of ROMS/BEC validation must be made available with supporting peer-reviewed publications in scientific journals. In pursuit of that objective, SCCWRP has produced three (3) recent publications, which do not yet prove the SCCWRP hypothesis, but are beginning to provide transparency on the computational details of the specific variant of ROMS/BEC model that SCCWRP is promoting. These recent ROMS/BEC publications by SCWWRP scientists are:

- Kessouri et al., (2021a) which provides a general science communication manuscript describing effects of land- and atmospheric nutrients on SCB nearshore productivity and biogeochemistry, published in the *Proceedings of the National Academy of Science (PNAS)*.
- Kessouri et al., (2021b) which describes architecture and primitive algorithms of the SCCWRP variant of the ROMS/BEC and gives example simulations of coastal eutrophication in a portion of the SCB and is published in the *Journal of Advances in Modeling Earth Systems (JAMES)*
- Ho, et al., (2021) which compares some previously published laboratory data on diffuser dilution by Roberts et al., (1989) compares with dilution predictions by the SCCWRP variant of ROMS/BEC

The Kessouri et al., (2021a) publication in *PNAS* provides links to the source code of the SCCWRP variant of ROMS/BEC found in a folder entitled <10.5281/zenodo.3988618>. These source codes were later updated by SCCWRP in a zip folder entitled <code_ap_2020.zip>.

3. Code Review of the SCCWRP Variant of ROMS/BEC:

Michael Baker International was retained by South Orange County Wastewater Authority (SOCWA) to evaluate the algorithms used in these codes, attempt to run the codes end to end and ultimately assess the efficacy of the SCCWRP variant of ROMS/BEC as a review of the available technology for plume tracking purposes. The updated source codes provided by SCCWRP in the zip folder <code_ap_2020.zip> contained 231 .F codes written in Fortran 90 codes and 57 .h header codes written in C. The header files contained C declarations and macro definitions to be shared between a number of different source files. Several versions of main ROMS/BEC program were found within the zip folder <code_ap_2020.zip>, including, <roms>, <roms_08> along with <Biology.F> and <ecosys_bec_LIANG.F>. These codes are written in "tungsten" Intel Fortran using MPI/Pro compiler. The results published Kessouri et al., (2021a & b) could not be reproduced because the codes must be run serially shuttling the output from one program to the

next in a sequence that has not been revealed to this reviewer. However, inspection of the architecture and algorithms of the ROMS/BEC ensemble of codes reveals that ROMS/BEC is a fixed-grid, split-explicit time-stepping oceanic model that solves the hydrostatic, free-surface equations of motion with Boussinesq approximations in a terrain-following grid system, (cf. **Figure 1**). While the terrain-following grid system in **Figure 1** is three dimensional, with a number of depth layers, a hydrostatic Boussinesq model like the SCCWRP variant of ROMS/BEC only produces 2-dimensional horizontal solutions in each depth layer. Such a model has no vertical dynamics such as vertical advection (upwelling currents) or vertical eddy diffusion. The SCCWRP variant of ROMS/BEC uses a K-profile parameterization (KPP) for turbulence closure. Turbulent mixing is calculated by a numerical hyper-diffusion related only to the horizontal advection (since the model has no vertical dynamics), with an effective diffusivity coefficient that decreases with the grid scale, as implemented previously by Uchiyama et al. (2014). However, these turbulent mixing algorithms are turned off within fixed mixing volumes prescribed around each outfall in order to represent the nearfield plume dilution. The ocean optics physics in the SCCWRP variant of ROMS/BEC is extremely primitive, in spite of the fact the full set of algorithms detailing the propagation of downwelling irradiance through the ocean water column has been well known and widely used for more than 100 years, (cf. Mie, 1908). These features of the SCCWRP variant of the ROMS/BEC codes give rise to two significant omissions which bias its results toward over stimulation of plankton growth rates and under-prediction of outfall dilution rates, both of which provoke algal blooms that contribute to acidification and hypoxia through the decay processes following bloom die off. These significant omissions are detailed in the following sub-sections.

3.1) Omission #1 No Backscattering Physics in Formulations of Light Attenuation:

Photosynthesis, phytoplankton growth rates, and biomass are controlled by the availability of nutrients (principally nitrates and ammonia) and solar irradiance in blue/green band of the visible light spectra, at wave lengths between $\lambda = 400$ nm and $\lambda = 700$ nm, referred to as photosynthetically available radiation, (PAR). It is no coincidence that photosynthetic organisms in the sea (e.g. phytoplankton) have evolved to the PAR band, as this is the deepest penetrating portion of the light spectra, (cf. **Figure 2**). Phytoplankton growth and survival is limited to the *Euphotic Zone,* which extends from the sea surface to the depth of penetration of incident light. While the euphotic zone may extend to depths of 200 m in the open ocean waters of the California Current, it typically does not exceed depths of 50 m in coastal waters, (approximately the depth of the deepest ocean outfalls in the Southern California Bight).

Mie Theory (cf. Mie, 1908) teaches that downwelling photosynthetically available solar irradiance, $PARz$, decays exponentially with depth, z, in the water column from a maximum level at the sea surface, $PARO$, according to:

$$PARz = PARO \exp\left[-C_d\, z\right] \qquad (1)$$

where C_d is the *diffuse attenuation coefficient*. The diffuse attenuation coefficient C_d is a complex function of a two primary light attenuation processes acting on various water column constituents,

(cf. **Figure 3**). Downwelling PAR attenuates due to the processes of *absorption* and *scattering*. Water molecules and dissolved organic matter (DOM) absorb downwelling PAR, while suspended

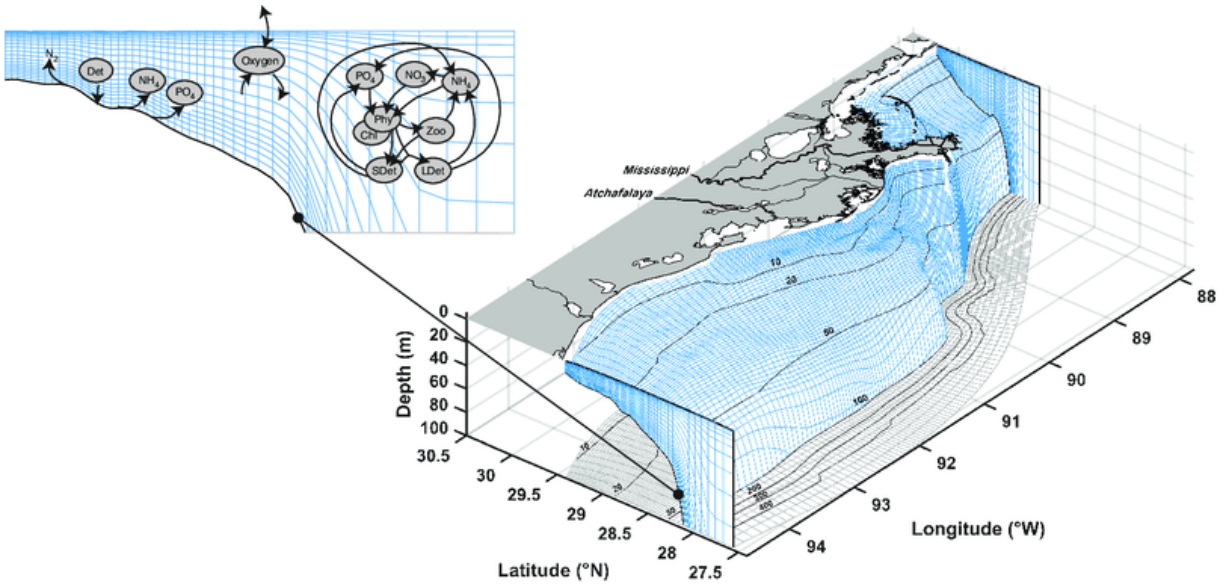

Figure 1: Schematic of a ROMS/BEC terrain-following grid, (from Fennel and Laurent, 2018).

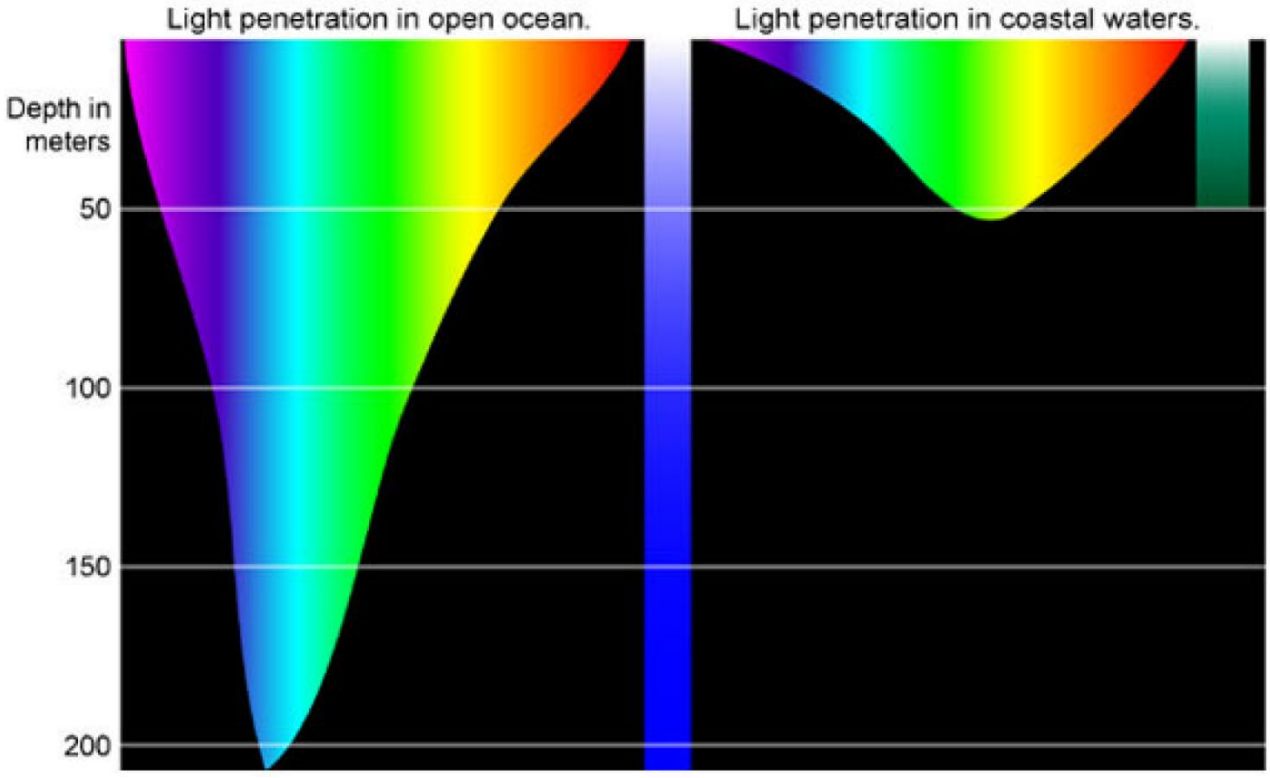

Figure 2: Schematic of depth of penetration of the visible light spectra in the ocean water column. Note that the blue/green band (PAR) is the deepest penetrating portion of the visible light spectra.

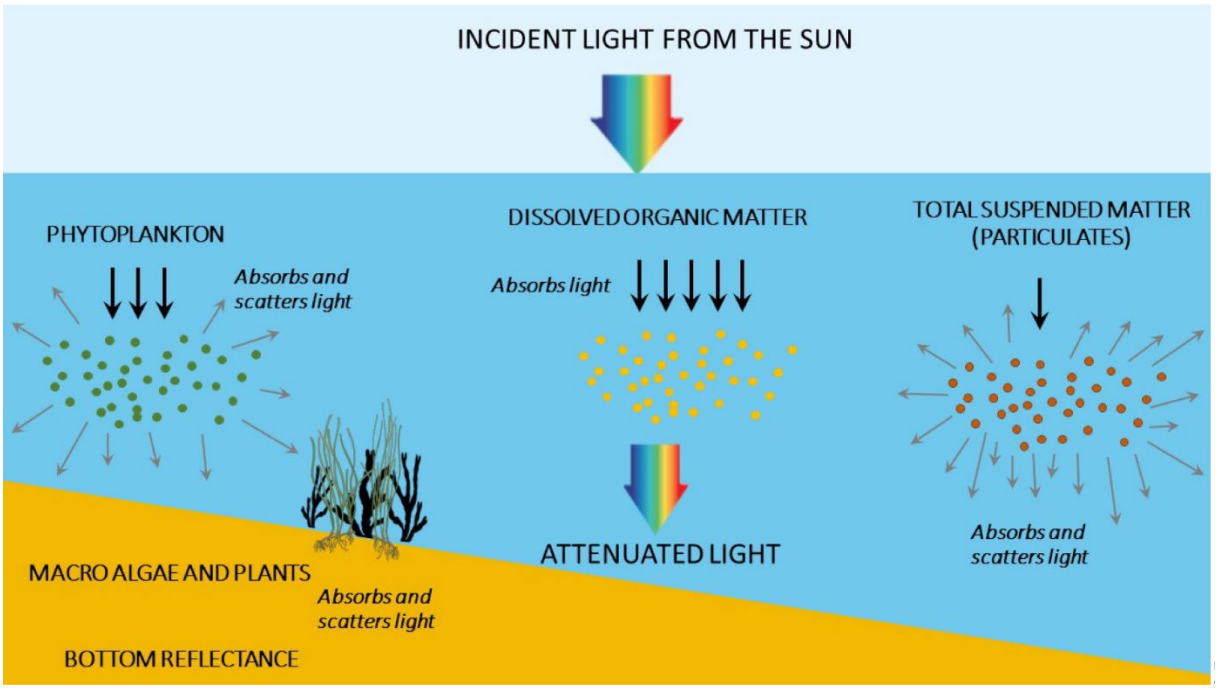

Figure 3: Schematic of light attenuation processes in the ocean water column.

particulate in the water column, including both inorganic dust and sediment particles and organic particulate such as plankton and detritus, both absorb and scatter downwelling PAR. The significance of scattering on photosynthetic rates and growth rates of plankton occurs when light is scattered back toward the sea surface, (referred to as back scattering). Back-scattering often results in abrupt, anisotropic reductions in downwelling PAR. In coastal waters where seabed depths are typically less than 50 m, even benthic plants and macro algae will absorb and scatter downwelling PAR. Consequently, the diffuse attenuation coefficient is a complex function of the abundance of these various absorbing and scattering water column constituents as represented generally by the formulation of Morel and Loisel (1998) according to:

$$C_d = \frac{a}{\cos\Omega}\left[1+\frac{b}{aB_0}\int_0^{\theta}\beta(N,k,\theta)d\theta\right]^{0.5} \qquad (2)$$

$$\text{where: } B_0 = \int_0^{\pi}\beta(N_0,k_0,\theta)d\theta \text{ at } z = 0$$

Here, Ω is the angle of down-welling light relative to the unit sea surface normal vector; a is the *absorption coefficient*; b *is the scattering coefficient*; and $\beta(k,N,\theta)$ is the *volume scattering function* normalized to spherical suspended particulate with non-dimensional particle diameter,

$k = D / 2\lambda$, where D is the physical particle diameter, and $N = f(D, z)$ is the particle number concentration (numbers of scattering and absorbing particles per unit volume), which is a function of depth and particle diameter; θ is the scattering (solid) angel in steradians; and B_0 is the total volume scattering function at the sea surface, integrated over all possible scattering directions between fully back scattered ($\theta = 0$) and fully forward scattered ($\theta = \pi$).

In contrast to equations (1) & (2), the formulation of attenuation of PAR with depth in the code for the SCCWRP variant of ROMS/BEC contains no scattering coefficient and no volume scattering function. Inspection of the PAR formulation in the ROMS/BEC codes (cf. the pink highlighted line of code in APPENDIX A) indicates that PAR attenuates with depth only by the effects of absorption by sea water molecules and absorption by phytoplankton according to:

PARz=PAR0*exp(-abs(z_r(i,j,k))*(kwater+kphyto*Phyt(k))) (3)

where Phyt(k) is the instantaneous phytoplankton concentration; kwater is the absorption coefficient of pure seawater that is assumed to be a constant, kwater = 0.04 per meter of depth; kphyto* Phyt(k) is the absorption coefficient of phytoplankton taken as 0.03[Phyt(k)] per meter of depth, and kwater+kphyto* Phyt(k) = *a* is the total absorption coefficient. By this formulation, the absorption coefficient becomes a highly simplified default version of the attenuation coefficient. There are no terms or variables in equation (3) to account for back scattering or absorption by other constituents in seawater such as dissolved organic matter (DOM), detritus particles and inorganic dust and sediment particles (cf. **Figure 3**). By this formulation, the light limiting effects on photosynthesis and plankton growth rates in the SCCWRP variant of ROMS/BEC occur only through absorption of PAR by seawater molecules and by the resident plankton population itself. This simplistic formulation of PAR attenuation originated with Fasham, et al., (1990) who referred to kphyto as the *phytoplankton self-shading parameter* (i.e., a descriptor for the phytoplankton absorption coefficient); and ever since, this formulation has been adopted without modification by a certain niche of ROMS/BEC modelers, (e.g., Uchiyama et al., 2014; Deutsch et al., 2021; Kessouri et al., 2021 a & b). When confronted with this concern at the 12 December 2022 code review meeting, the SCCWRP modelers insisted their PAR attenuation formulation did include back scattering effects, citing Fasham, et al., (1990) to support that claim; and yet equation (4) in Fasham, et al., (1990) and the pink highlighted line of code in APPENDIX A teaches otherwise. Furthermore, it is impossible to account for back scattering without calculating the volume scattering function, $\beta(k, N, \theta)$, and it is impossible to calculate the volume scattering function without inputs for particle diameter, k, and particle number concentration , N. The codes for the SCCWRP variant of ROMS/BEC contain no such algorithms or inputs.

These are significant omissions because back scattering by tiny suspended particulate in coastal waters (particle sizes in the range of 0.1 μm $\leq D \leq 1$ μm) accounts for 66% to 75% of the total attenuation of PAR in coastal waters, (cf. panels a & c vs. panels b & d in **Figure 4**), while absorption attenuates only the remaining 25% to 33% of the downwelling irradiance in the PAR

band (cf. Petzhold, 1972, Hammond, et al., 1995; and Lee et al., 2004). Furthermore, by admitting only to absorption by phytoplankton, while neglecting absorption by other seawater constituents such as colored dissolved organic matter (CDOM) and suspended sediment, the SCCWRP formulation in equation (3) above (adopted from Fasham, et al., 1990) is only accounting for a third or less of the total absorption across the PAR band, (cf. panels b & d in **Figure 4**). Therefore, if only the absorption coefficients for plankton and seawater molecules are used as a proxy for total diffuse attenuation coefficient, that approximation (as invoked in the SCCWRP variant of ROMS/BEC codes) will under-estimate the diffuse attenuation coefficient in coastal waters by a factor of approximately 20, (cf. **Figure 5**). Again, that approximation originated with Fasham, et al., (1990) who were applying it to deep water oceanic environments, where it may not be such a bad approximation; but SCCWRP is now juxtaposing it to coastal waters where **Figures 5 & 6** indicate it is a bad approximation due to the abundance of additional absorbing and strongly back-scattering seawater constituents.

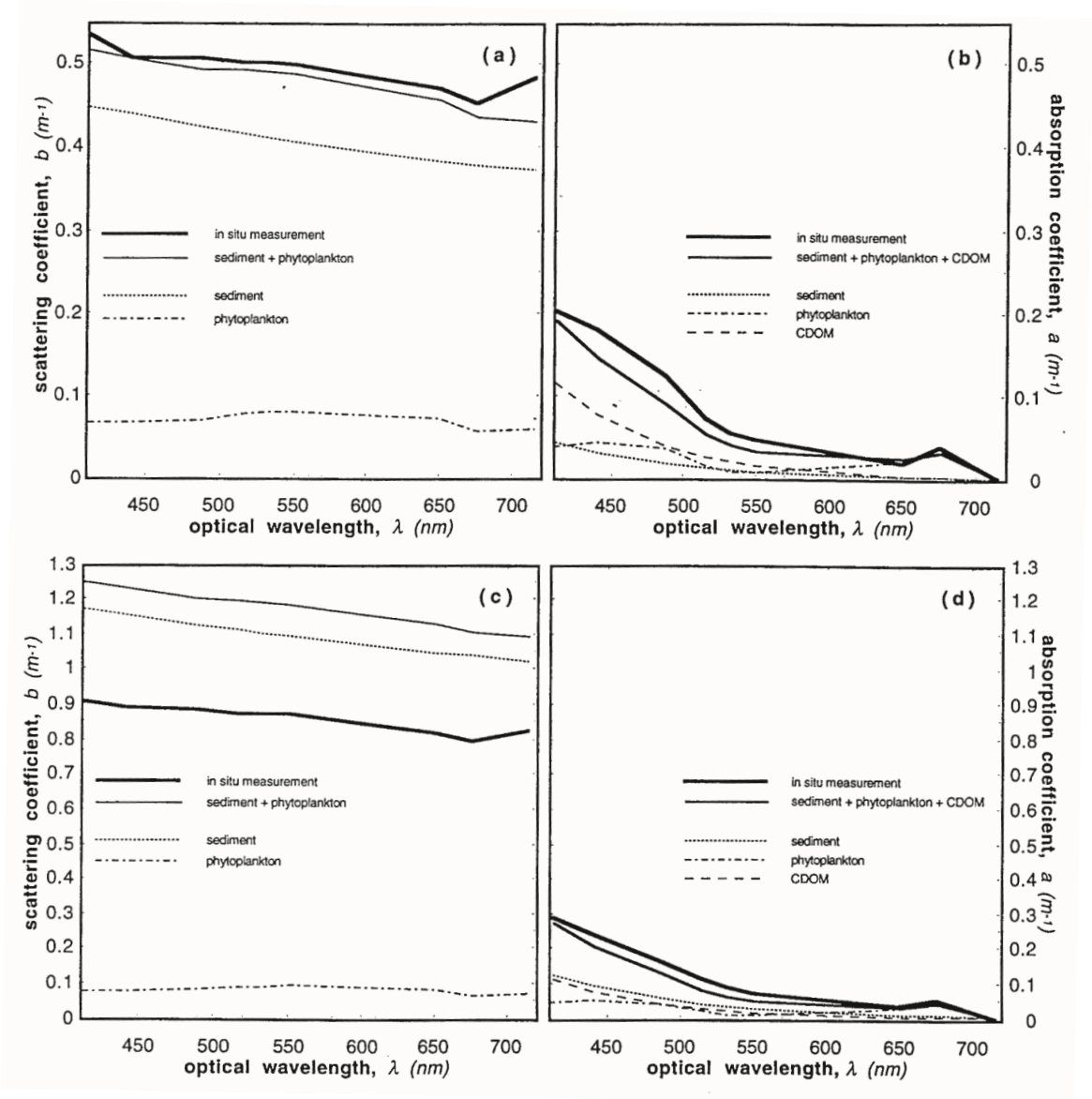

Figure 4: Measured scattering coefficients, *b*, (left) and absorption coefficients, *a*, (right) in coastal waters offshore of Oceanside, CA. Note scattering coefficients are more than 2-3 times greater than absorption coefficients across the PAR band. Data measured with a WetLabs absorption/attenuation meter, (from Hammond et al., 1995).

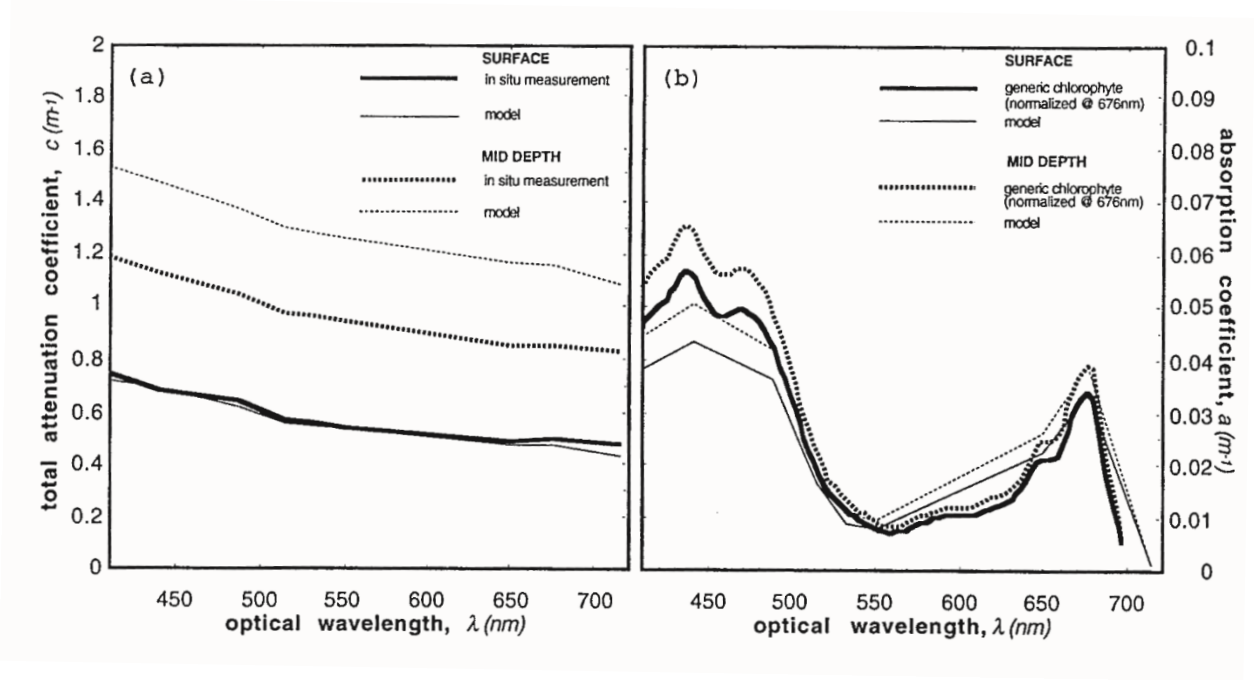

Figure 5: Measured total diffuse attenuation coefficients, C_d, (left) and absorption coefficients, *a*, (right) in coastal waters offshore of Oceanside, CA. Note that if only the absorption coefficient for plankton is used as a proxy for total diffuse attenuation coefficient, that approximation will under-estimate the diffuse attenuation coefficient by a factor of approximately 20. Data measured with a WetLabs absorption/attenuation meter, (from Hammond et al., 1995).

Figure 6 compiles and maps thousands of diffuse attenuation measurements off the North Atlantic and Mediterranean coasts of Europe. Inspection of **Figure 6** indicates the diffuse attenuation coefficient increases from as little as $C_d \cong 0.45$ in the deep water oceanic environments offshore (comparable to what SCCWRP has assumed for the absorption coefficients of seawater molecules and phytoplankton); but increases to as much as $C_d \cong 1.96$ everywhere in the coastal waters along the open coastline of Europe and in most places in the coastal waters of the Mediterranean Sea. Therefore, **Figure 6** indicates that the approximation SCCWRP has made by applying an oceanic formulation (that omits back-scattering and absorption by seawater constituents other than plankton) to coastal waters will underestimate the diffuse attenuation coefficient by a factor of 44, or more than twice the estimated error indicated by the Oceanside attenuation coefficient measurements in **Figure 5**. Omission of back scattering and absorption by sea water constituents other than phytoplankton in the formulation of available PAR leads to calculations of a deeper photic zone with higher PAR intensity at any given depth, both of which result in higher photosynthetic rates and growth rates than would otherwise occur

in coastal waters. Consequently, the photosynthetic rates and plankton growth rates that SCCWRP has been calculating in the inner Southern California Bight are over-stimulated by excessive PAR intensity and extend depths of the euphotic zone to where there would otherwise be insufficient PAR for any photosynthesis or phytoplankton growth to occur in Nature.
To correct the over-simplified ocean optics formulations of PAR attenuation in the photosynthetic and growth rate portions of the codes for the SCCWRP variant of ROMS/BEC, the codes must be expanded to solve the full set of *Mie Scattering* algorithms to obtain solutions for the *scattering coefficient*, *b*, and the *volume scattering function,* $\beta(k, N, \theta)$. This will also require gathering additional data on suspended sediment (particle) concentrations and particle size distributions of the suspended sediment using a *laser particle sizer*. These data should be acquired for both the offshore ocean background levels and the river discharges. The most efficient scattering and absorbing particles at PAR wave lengths are in the size regime of clay and fine silt particulate, for which the particle number concentration varies with particle diameter and depth according to a hyperbolic distribution (Bader, 1970; Kirk, 1983) given by:

$$N = f(D,z) = N_1(z)\, D^{-\gamma} \text{ where } \quad 0.7 \le \gamma \le 6.0 \qquad (4)$$

In this hyperbolic distribution, $N_1(z)$ is the particle number concentration in the smallest size decade, which varies with depth, and typically represents particle sizes in the range of 0.1 μm $\le D \le 1$ μm; while γ is the slope of the particle size distribution on a logarithmic sale. These tiny particles become increasingly important the closer the modeling grids are extended towards the coastline, where coastal rivers and non-point-source runoff from beach and bluff erosion dump millions of tons of micron-size, fine-grained sediment as wash-load into the Southern California Bight each year (Inman and Jenkins, 1999; Jenkins and Inman, 2006). Not only does clay particulate in wash-load transport significant quantities of adsorbed nutrients into coastal waters, but these tiny particles have remarkably slow settling velocities, in spite of a tendency to flocculate in seawater (cf. Sverdrup, 1942; Mehta & Partheniades, 1975; Aijaz & Jenkins, 1993, 1994). For example, **Table 1** indicates that clay particles smaller than 2 microns settle less than a foot per day, while **Figure 7** shows how fine-grained silts and clays discharged from rivers and streams during wet weather can spread across nearly the entire SCB as a result of these very slow settling rates, even during La Nina drought years such as 1975. Due to a lower immersed weight, similar sized nano-plankton and detrital particulate settle even more slowly. In either case, the settling velocity of micron-size inorganic and organic particulate is smaller than the *gradient eddy diffusivity velocity* in the mixed layer of the coastal ocean, cf. Armi, (1979). Consequently, the most aggressive PAR scattering and absorbing particulate can remain indefinitely in suspension in coastal waters and will not simply settle out of suspension following major storm and flood events. Once introduced, the only mechanism that removes suspensions of micron-sized particulate from the near-shore waters is advection by coastal current systems.

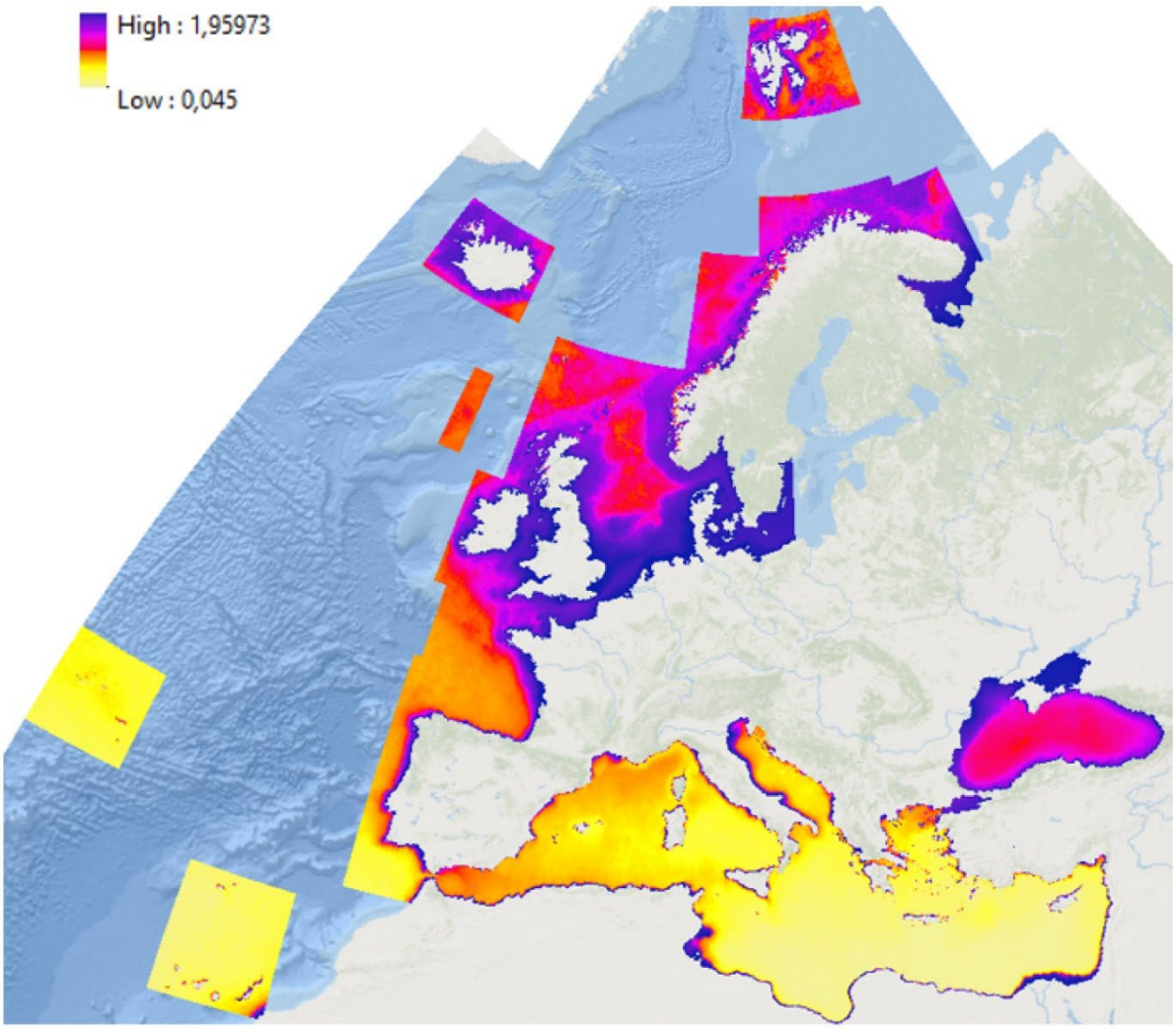

Figure 6: Diffuse attenuation coefficient, C_d, in the PAR band for European waters, at 100m resolution. Dark blue/violet colors correspond to highest attenuation of PAR, ($C_d \sim 1.959$), while yellow colors correspond to lowest attenuation of PAR, ($C_d \sim 0.045$). Note that the diffuse attenuation in coastal waters along the open coastline of Europe is approximately 44 times greater that in the oceanic waters further offshore, (from Frigstad and King, 2020).

Table 1: Settling velocity data of quartz sediment in ocean water, after Sverdrup et al., (1942)

	Particle Diameter	Size Parameter	Time to Fall 10cm				Settling Velocity
	(μm)	*k_{530} (μm)*	*(days)*	*(hours)*	*(minutes)*	*(seconds)*	*(m/day)*
clay	0.12	0.11	87	3	19		0.001
	0.25	0.23	21	18	50		0.004
	0.49	0.45	5	10	42		0.018
	0.98	0.91	1	8	41		0.074
	1.95	1.81		8	10		0.3
silt	3.9	3.9		2	2	32	1.2
	7.8	7.2			30	38	4.7
	15.6	14.5			7	40	18.8
	31.2	29			1	55	75.2
	62.5	58				29	301
very fine sand	125	116				8.3	1040
fine sand	250	232				2.7	

Figure 7: LANDSAT multi-spectral scanner image of suspended particulate across the Southern California Bight due to dispersion of river wash load particulate following a Pacific storm on 14 March 1975.

3.2) Omission #2 Non-calibrated Schematization of Ocean Outfall Discharges:

The SCCWRP variant of ROMS/BEC is a fixed grid, hydrostatic Boussinesq model that is only capable of generating a collection of 2-dimensional horizontal solutions in discrete depth layers stacked one on top of the other between the seabed and the sea surface. As such it has no vertical dynamics, making it ill-suited for resolving the large local vertical velocities associated with the freshwater discharges from the bottom-mounted diffusers of municipal ocean outfalls. Furthermore, because vertical mixing of the buoyant wastewater effluent occurs on a scale smaller than the grid resolution of the SCCWRP variant of ROMS/BEC, it was necessary in the SCCWRP variant of ROMS/BEC to assume a fixed, time-invariant mixing volume in order to represent the outcome of nearfield initial mixing and dilution within the outfall plume. Consequently, the SCCWRP variant of ROMS/BEC is incapable of simulating what actually occurs in nature where the mixing volume varies continuously with changes in temperature/salinity profiles, winds, waves, currents and outfall discharge rates, as well as with individual outfall specific parameter such as diffuser length, numbers and size of discharge ports. This limitation cannot be corrected in a fixed-grid hydrostatic model even by using very fine grid scales. Also, there is an obvious issue with whether the scale separation between the variable circulation in the farfield and the nearfield plume mixing volume is actually valid. Even with very fine scale model resolution this assumption will fail, and the turbulence of the outfall plume must be calculated explicitly, as is typically done with EPA certified plume models such as Visual Plumes (UM3) and its most recent ugrade, Plumes 20 UM3.

In an attempt to work around these intrinsic difficulties and limitations, the SCCWRP variant of ROMS/BEC parameterized the assumed mixing volume using a formulation lifted from Uchiyama et al., (2014) that is based on the product of 2 shape functions, namely: A(x,y) which specifies the horizontal footprint of the plume, and H(z) which specifies the vertical shape of the plume. The shape function A(x,y) merely specifies the number of horizontal grid cells that are assumed to enclose the plume. That means the horizontal footprint of the plume is an assemblage of 300 m squares. All of the observations of outfall plume footprints in Nature (as well as in laboratory miniatures) are either elliptic, tear-dropped or other assortments of complex curvilinear shapes. The vertical shape function, H(z), in the ROMS/BEC codes was based on a Gaussian functional identical to that in equation (5) of Uchiyama et al. (2014), which uses two (2) parameters that were assumed to be the same for all outfalls in Kessouri et al., (2021b). This SCCWRP publication references Uchiyama et al. (2014) for how the two parameters in the vertical shape function, H(z), were determined; and in turn, Uchiyama et al. (2014) references the laboratory measurements by Roberts et al. (1989), made around a miniature diffuser in a flume, as the method by which the two parameters in the vertical shape function were determined. This approach is corrupt because laboratory miniatures cannot reproduce the turbulent mixing that occurs with prototype scale diffusers in Nature. The laboratory miniatures are scaled by the Froude number whereas turbulent mixing scales by the Reynolds number and it is impossible to simultaneously scale both the Froude number and the Reynolds number in a laboratory miniature.

Since the work of Ho et al. (2021) had been featured prior to publication at the ROMS/BEC *Validation and Scenarios Subcommittee Meeting* held at SCCWRP in September 2019, it was at first believed that both the horizontal shape function and the two parameters in the vertical shape function were imported from the Ho et al, 2021 publication, because she based her work on the same laboratory measurements in Roberts, et al. (1989) that Uchiyama et al. (2014) had used. However, it was later learned at the 12 December 2022 code review meeting at SCCWRP that their ROMS/BEC did not use the results from Ho et al., 2021 to determine the mixing volume shape functions or its associated free parameters. Hence the Ho et al. (2021) paper is actually a *red herring* that in no way serves to establish the efficacy of the SCCWRP variant of ROMS/BEC. Consequently, there are actually only two peer-reviewed papers of the SCCWRP variant of ROMS/BEC in existence at this time, namely: Kessouri et al., (2021a & b).

Lines of ROMS/BEC code that explicitly identify how the mixing volume shape functions and its associated free parameters could not be found anywhere among the 231 Fortran -90 and 57 header C-codes that were reviewed. What was learned at the 12 December 2022 code review meeting at SCCWRP is that the two mixing volume shape functions and its free parameters were derived from "CDOM data contained in outfall monitoring reports". The details of how that was actually accomplished was never disclosed in Kessouri et al., (2021b) and still remain a mystery at the time of this writing. However, Kessouri et al., (2021b) states the same parameters in the vertical shape function were used for all the outfalls they modeled; which amounts to an assumption that one size fits all outfalls, both large and small. This unrealistic assumption is further compounded by the fact that the vertical cross-section of a prototype outfall plume does not follow a Gaussian distribution. **Figure 8** plots Plumes-20 (UM3) solutions for the variations in mixing volume of the San Elijo Ocean Outfall in response to seasonal variations in temperature/salinity profiles, winds, waves, currents, discharge rates. Note that the vertical variation in the size of the mixing volume is not Gaussian as assumed in the present formulation of the SCCWRP variant of the ROMS/BEC; and that the size of the volume varies significantly with depth and has a strong seasonal variance.

There is also reason to doubt the efficacy of extracting the two mixing volume shape functions and its free parameters from the kind of CDOM data typically available in monitoring reports. Recent plume tracking field studies using an Iver3 autonomous underwater vehicle (AUV) measuring fDOM as a plume tracer (the portion of CDOM that fluoresces) indicate that fDOM measurements must be closely spaced, no more than 100 meters between measurements, in order to avoid spatial aliasing by natural variations in ambient background concentrations of fDOM, (cf. Jenkins and Shatila, 2022). The typical patterns of NPDES monitoring stations in outfall monitoring reports are much more widely spaced than 100 m. Furthermore, the evidence that is emerging from these AUV plume tracking field studies indicate that nutrients discharged from ocean outfalls in the lower SCB dilute much faster in the nearfield of the outfalls than the SCCWRP variant of ROMS/BEC seems to predict. These AUV plume tracking field studies find that the dilution rates at the Encina Ocean Outfall (EOO) are extremely high even when discharging near maximum permitted discharge rates. At the EOO, the AUV collected 68,538 separate measurements of fDOM along a total distance surveyed of 21.2 km. The fDOM heat map generated from these 68,538 measurements of fDOM concentrations is plotted in **Figure 9**.

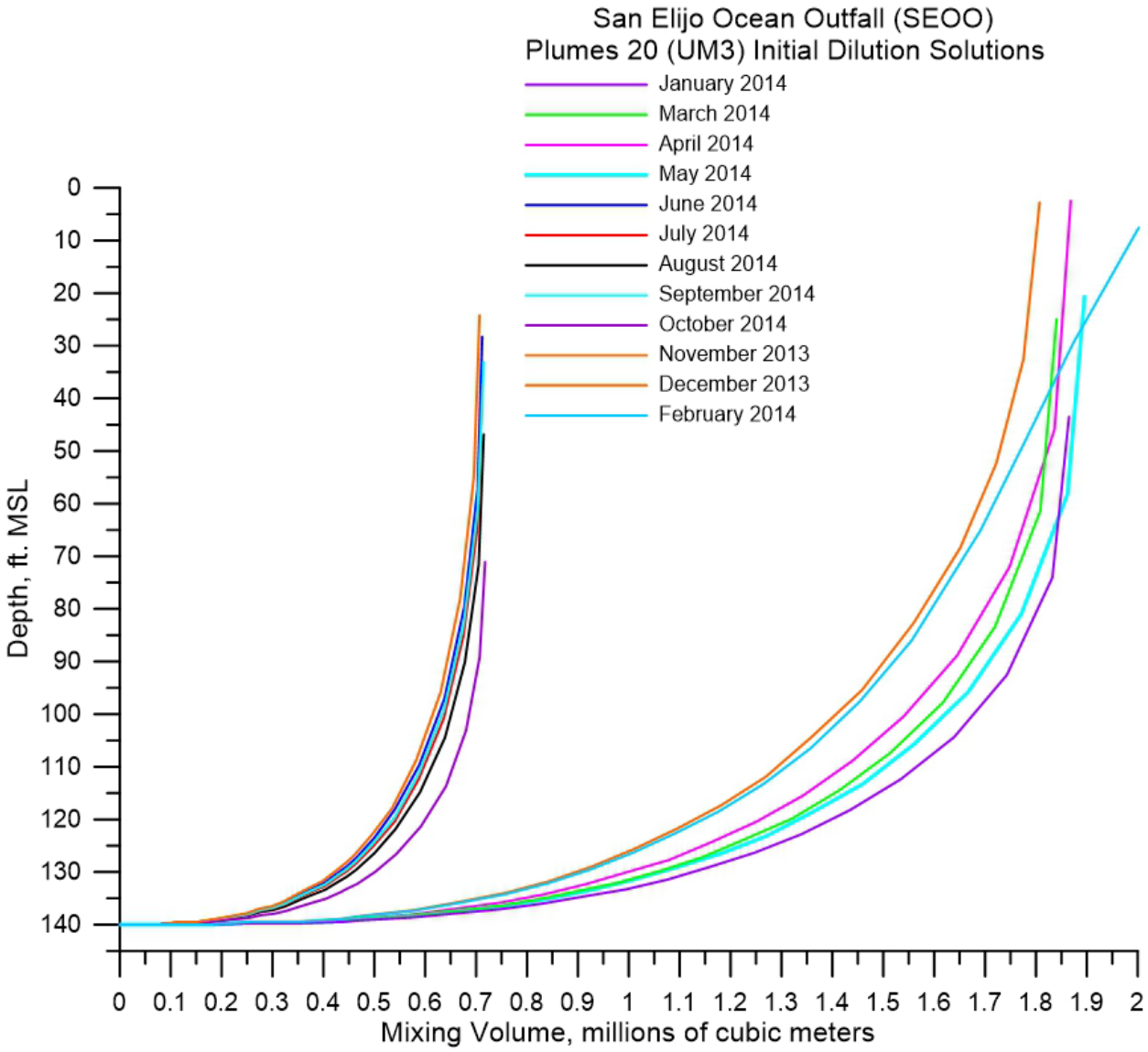

Figure 8: Plumes-20 (UM3) solutions for the variations in mixing volume of the San Elijo Ocean Outfall in response to seasonal variations in temperature/salinity profiles, winds, waves, currents, discharge rates. Note that the vertical variation in the size of the mixing volume is not Gaussian as assumed in the present formulation of the SCCWRP variant of the ROMS/BEC.

Inspection of **Figure 9** reveals that variations in fDOM concentrations across all depths surveyed by the AUV range from $fDOM_{(x)}$ = 0.2 ppb to 1.3 ppb. These fDOM variations during ebb tide exhibit horizontal structures having high spatial coherence with the EOO diffuser, with a singular, large fDOM feature centered 393.9 m down-drift (south) of the EOO diffuser in which elevated fDOM are in the range of $fDOM_{(x)}$ = 0.7 ppb to 1.3 ppb, or 136% to 339% higher than the depth-averaged natural background fDOM concentration $fDOM_{(\infty)}$ = 0.296 ppb. The fDOM heat map in **Figure 9** is converted into a signal to noise ratio heat map in **Figure 10** to convert the fDOM concentrations in **Figure 9** into corresponding SNR_{fDOM} patterns. Inspection of **Figure 10** reveals that the signal to noise ratio of the suspected plume remnant ranges from $SNR_{fDOM} \cong 1.1$ along its outer perimeter, to as high as SNR_{fDOM}= 3.39 in its inner core 393.9 m downstream of the EOO diffuser. Therefore, the elevated fDOM concentrations found in this feature satisfy the lowest order significance threshold for detection, (i.e., $SNR_{fDOM} \geq 1$). To assess minimum dilution levels in the EOO plume remnant, the SNR_{fDOM} heat map in **Figure 10** was transposed into a dilution heat map in **Figure 11** on the basis that the initial fDOM concentration at the point of discharge is $fDOM_{(x=0)}$ = 217.5 ppb. Regions of high SNR in **Figure 10** will correspond to regions of low dilution values relative to the dilution elsewhere within the AUV survey area. **Figure 11** indicates that the dilution factor (D_{fDOM}) for the fDOM features would be no less than as D_{fDOM} = 215:1 in the inner core of the plume remnant, or a factor of 1.5 times greater than the assigned minimum initial dilution of Dm = 144:1 established in the current NPDES permit (No. CA0107395; Order No. RS-2018-0059). The dilution along the outer perimeter of the plume remnant ranges from D_{fDOM} = 666:1 to as much as 15,000:1. Elsewhere in the wake of the EOO diffuser dilution ranges from D_{fDOM} = 35,000:1 to 75,000:1 so that any nutrients (nitrates or ammonia) in the EOO effluent would be below quantifiable detection limits for any plume remnants beyond 400 m from the outfall. These findings directly contradict the those of the simulations from SCCWRP variant of ROMS/BEC that were published in Kessouri et al., (2021b).

In summary the calculation of the outfall dilutions in the ROMS/BEC is corrupt because, 1) it is based on a fixed, time-invariant mixing volume which never occurs in Nature (an assumption critiqued even by Uchiyama et al., 2014); 2) the shape functions that define the size and shape of the mixing volume do not replicate the size and shape of outfall plumes in Nature; the horizontal footprint of a prototype outfall plume does not resemble rectangular shapes, and the vertical cross-section of a prototype outfall plume does not follow a Gaussian distribution; and 3) the mixing volume of a prototypic scale outfall plume in Nature varies continuously over time in response to the vertical variations in temperature/salinity profiles, winds, waves, currents and outfall specific parameters such as discharge rates, diffuser length, numbers and size of discharge port; none of which the ROMS/BEC formulation of the mixing volume can replicate or even adequately approximate. As a result, the SCCWRP variant of ROMS/BEC under predicts the dilution that occurs in the modeled outfall plume which in turn leads to higher undiluted nitrate and ammonia concentration in the plumes, thereby imparting a bias in favor of excessive plankton photosynthetic rates and growth rates stimulated by the exaggerated nutrient concentrations in both the nearfield and farfield of the outfall plumes.

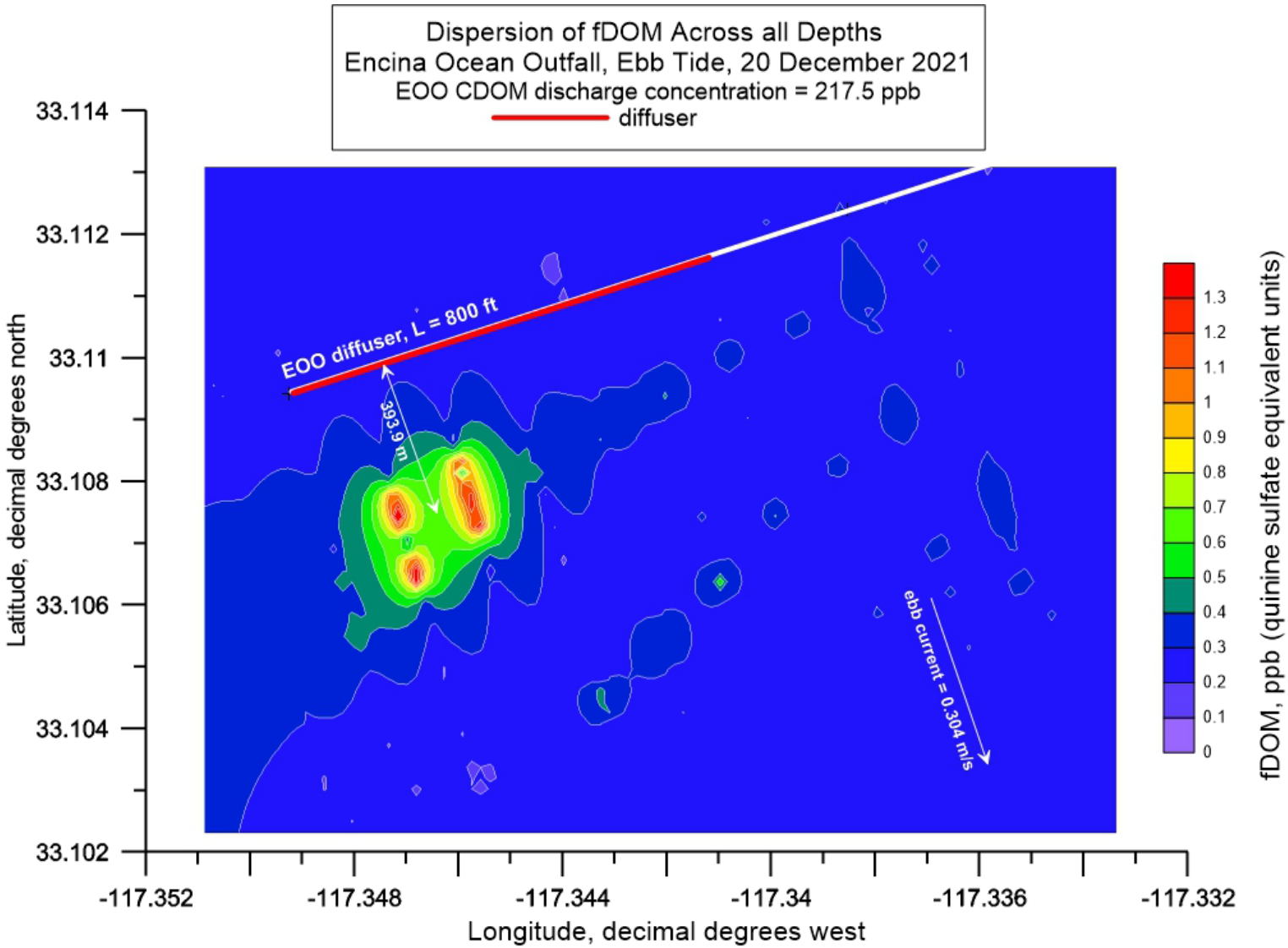

Figure 9: Full depth contour plot (aka, heat map) of AUV measurements of fDOM during surveys of the discharge plume from EOO during ebb tide on 20 December 2021. Average EOO discharge rate =31.20 mgd during ebb tide; End-of-pipe discharge concentration of fDOM = 217.5 ppb (QSU); End of pipe salinity = 0.96 psu; Trapping level (pycnocline depth) = -13.1 ft MSL; Mean ebb tide current = 0.304 m/s (0.59 kts) toward the southeast.

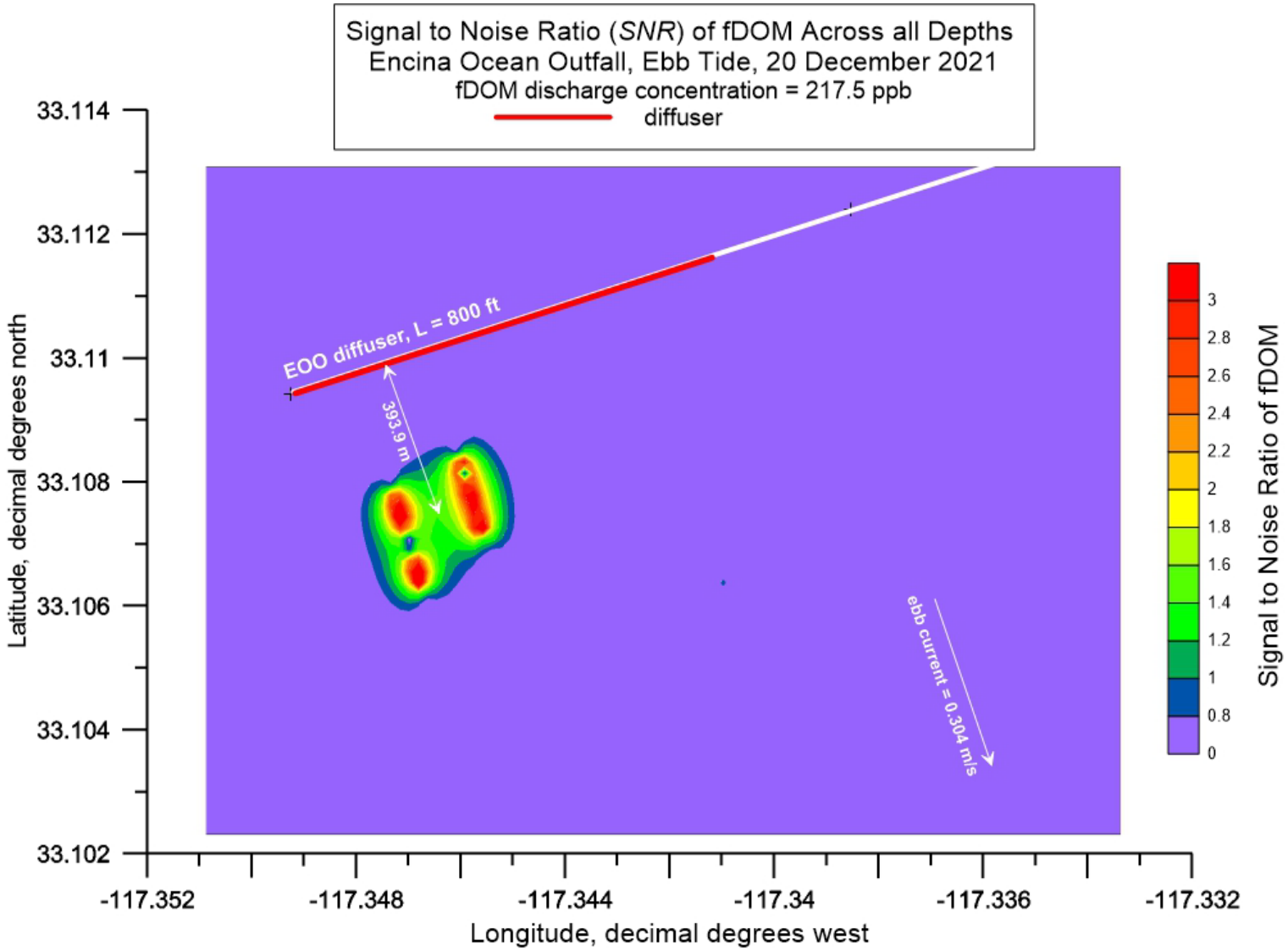

Figure 10: Full depth contour plot (aka, heat map) of the Signal to Noise Ratio (SNR) of fDOM during AUV surveys of the discharge plume from EOO during ebb tide on 20 December 2021. Average EOO discharge rate =31.20 mgd during ebb tide; End-of-pipe discharge concentration of fDOM = 217.5 ppb (QSU); End of pipe salinity = 0.96 psu; Trapping level (pycnocline depth) = -13.1 ft MSL; Mean ebb tide current = 0.304 m/s (0.59 kts) toward the southeast.

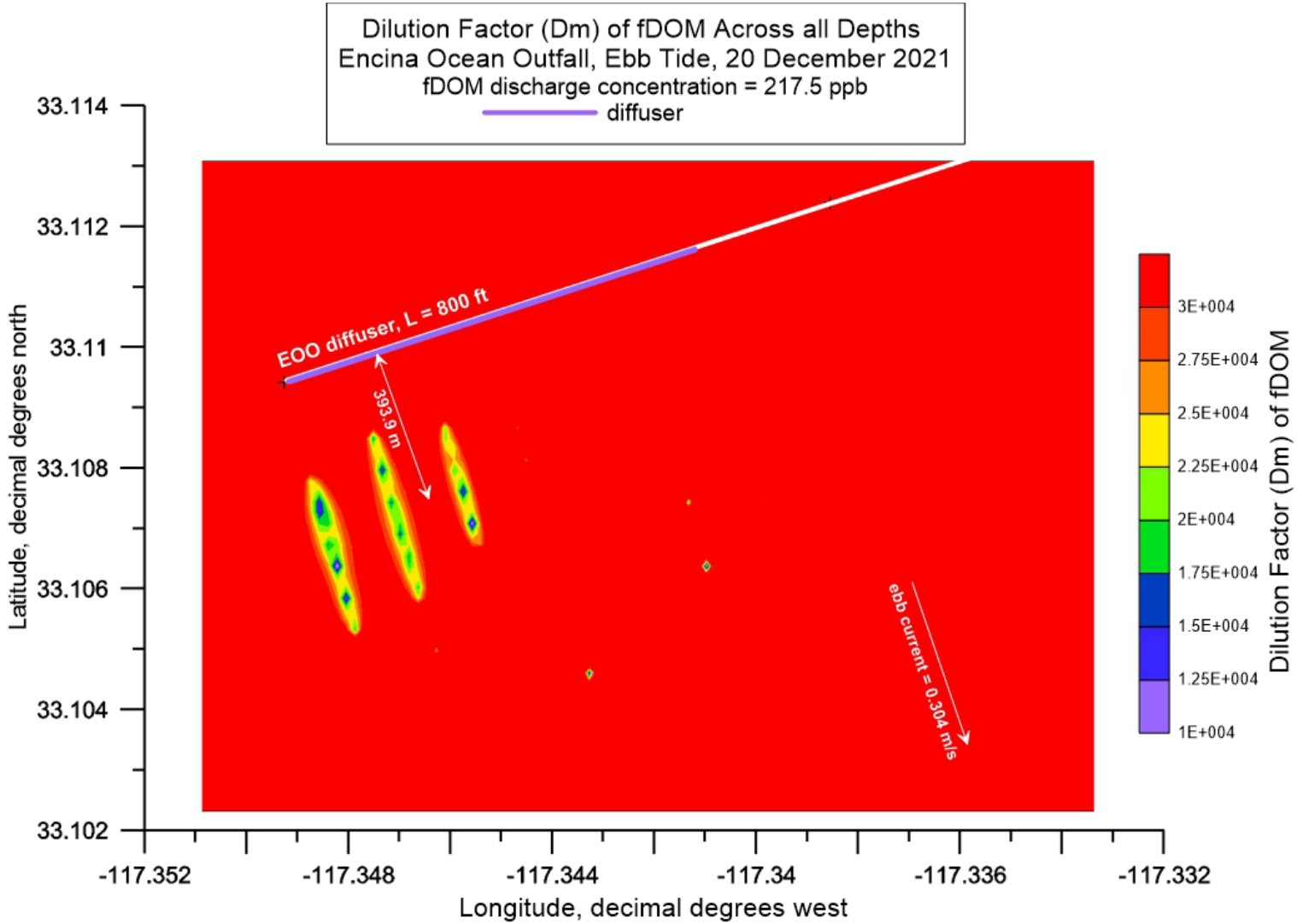

Figure 11: Full depth contour plot of the (aka, *heat map*) dilution factor (D_{fDOM}) of fDOM during AUV surveys of the discharge plume from EOO during ebb tide on 20 December 2021. Average EOO discharge rate =31.20 mgd during ebb tide; End-of-pipe discharge concentration of fDOM = 217.5 ppb (QSU); End of pipe salinity = 0.96 psu; Trapping level (pycnocline depth) = -13.1 ft MSL; Mean ebb tide current = 0.304 m/s (0.59 kts) toward the southeast.

The embedded singularity imposed by the fixed mixing volume around the outfalls in the SCCWRP variant of ROMS/BEC can create numerical instabilities in the nutrient dispersion and plankton growth simulations. In order for the ROMS/BEC model to produce temporally stable solutions, the longest time step interval that can be used is limited by the *Courant-Friedricks-Lewy* (CFL) *Stability Criteria* (cf. Gallager et al., 1981) according to:

$$\Delta t \leq \frac{\Delta x}{\sqrt{2gh}} \tag{5}$$

where Δx is the grid cell horizontal dimension, h is the depth of the seabed, and g is the acceleration of gravity. The original ROMS-tar codes authored by Deutsch and Frenzel (that operated on computational domains well seaward of the municipal outfalls, cf. Deutsch et al., 2021) incorporated a safeguard against development of CFL numerical instabilities, (cf. **APPENDIX B**). In order to compute vertical advective fluxes of nutrients occurring at significantly higher rates than horizontal fluxes (as would occur near municipal outfalls), the ROMS-tar algorithms were designed to be free of the CFL criterion by allowing integration bounds for semi-Lagrangian advective flux to use as many grid boxes in upstream direction as necessary. Those CFL safeguards were prescribed within the fixed grid, hydrostatic architecture of the ROMS-tar model domain. However, the SCCWRP variant of ROMS/BEC applies a nonhydrostatic discretization within in its parameterized mixing volume surrounding the outfalls. In so doing, the CFL numerical instability safeguards do not function within those embedded singularities imposed by the fixed mixing volume around the outfalls. For a deep outfall like the Hyperion 5-Mile Outfall, (where the depth is on the order of $h = 60$ m), the SCCWRP variant of ROMS/BEC running on a horizontal grid resolution of $\Delta x = 300$ m would have to run at time steps no longer than $\Delta t \leq 8.76$ sec to avoid CFL numerical instabilities. Instead, the SCCWRP variant of ROMS/BEC was run in the Santa Monica Bay/San Pedro Shelf simulations in Kessouri et al., (2021b) at time steps of $\Delta t = 30$ sec. This excessive time step interval could explain the spurious results obtained in the third panel on the right-hand side of **Figure 2** in Kessouri et al., (2021b), cf. **APPENDIX C.**

4. References

Armi, L. A., 1979, “Effects of variations in eddy diffusivity on property distributions in the oceans,” Jour. Mar. Res., v.37, n.3, p. 515-530.

Bader, H.: 1970, The Hyperbolic Distribution of Particle Sizes*, J. Geophys. Res*., Vol. 75, pp. 2822-2830.

Baumgartner, D. J., Frick, W. E., and Roberts, P. J. W. (1994). "Dilution Models for Effluent Discharges (Third Edition)." U.S. Environmental Protection Agency, Office of Research and Development. EPA/600/R-94/086

Deutsch, C., Frenzel, H., McWilliams, J. C., Renault, L., Kessouri, F., Howard, E., et al. (2021). Biogeochemical variability in the California Current System. *Progress in Oceanography*, 102565.

Doneker, R. L., and Jirka, G. H. (1999). “Discussion of mixing of inclined dense jets” by Roberts, P. J. W., Ferrier, A., and Daviero, G.” (1997).” J. Hydraul. Eng., 125(3), 317–319.

Doneker, R. L. and Jirka, G. H. (2017). “CORMIX User Manual.” MixZon, Portland, Oregon. Updated February 2017.

Fennel, K., and A. Laurent, 2018, “N and P as ultimate and proximate limiting nutrients in the northern Gulf of Mexico: Implications for hypoxia reduction strategies”, *Biogeosciences*, vol 15, no. 10, p. 3121 – 3131, doi: 10.5194/bg-15-3121-2018.

Frick, W.E., Roberts, P., Davis, L., Keyes, J., Baumgartner, D., George, K., 2003, “Dilution models for effluent discharges, Forth Addition”, U.S. Environmental Protection Agency, Standards and Applied Science Division Office of Science and Technology, 148 pp.

Frick, W. E. (2004). "Visual Plumes mixing zone modeling software." Environmental Modelling & Software, 19, 645-654.

Frick, W., Ahmed, A., George, K., Laputz, A., Pelletie, G., and Roberts, P. (2010). "On Visual Plumes and Associated Applications." MWWD 2010 6th InternationalConference on Marine Waste Water Discharges and Coastal Environment, C. Avanzini, ed. Langkawi, Malaysia.

Frick, W. E., and Roberts, P. J. W. (2016). "Visual Plumes 2016: An Updated Public-Domain Plume Model Suite." Proc., International Symposium on Outfall Systems,ISOS2016, IWA. 10 - 13 May 2016.

Frigstad, H. and A. King, (2020), “Increased light attenuation in Norwegian coastal waters”,

Gallagher, R., H., 1981, *Finite Elements in Fluids*, John Wiley & Sons, New York, 290 pp.

Hammond, R. R., S. A. Jenkins, J. S. Cleveland, J. C. Talcott, A. L. Heath, J., Wasyl, S. G. Goosby, K. F. Schmitt & L. A. Leven, 1995, "Coastal water clarity modeling feasibility study," SAIC, Technical Report 01-1349-03-4841-000, 491 pp.
https://www.researchgate.net/publication/235097558_Coastal_Water_Clarity_Modeling_Feasibility_Study

Ho, M., Molemaker, J., Kessouri, F., McWilliams, J., and T. Gallien, 2021, “High-resolution nonhydrostatic outfall plume Modeling: Cross-Flow Validation”, *J. Hydraul. Eng.*, vol.147, No.8, 13 pp. doi 10.1061/(ASCE)HY.1943-7900.0001896

Inman, D. L., S. A. Jenkins & J. Wasyl, 1998, "Database for streamflow and sediment flux of California rivers," *University of California, San Diego*, Scripps Institution of Oceanography, SIO Reference Series 98-9, 13 pp. + 3 tbls. + 19 figs. + 4 appens.(v. 16; B-157) http://repositories.cdlib.org/sio/cmg/1/

Inman, D. L. & S. A. Jenkins, 1999, "Climate change and the episodicity of sediment flux of small California rivers," *Jour. Geology,* v. 107, p. 251–270. https://doi.org/10.1086/314346

Jenkins, S., and M. Shatila, 2022, "Plume Tracking Field and Model Analysis of Discharges from the Encina Ocean Outfall and San Elijo Ocean Outfall", submitted to San Elijo Joint Powers Authority and the Encina Wastewater Authority, 7 October 2022, 239 pp.

Kessouri, F., McLaughlin, K., Sutula1, M., Bianchi D. , Ho, M., McWilliams, J., Renault, L, Molemaker, J., Deutsch, C., and A. Leinweber, 2021a, "Coastal eutrophication drives acidification, oxygen loss, and ecosystem change in a major oceanic upwelling system", *Proceedings of the National Academy of Science,* vol. *118*, No. 21, 8 pp., doi.org/10.1073/pnas.2018856118

Kessouri, F., McLaughlin, K., Sutula1, M., Bianchi D. , Ho, M., McWilliams, J., Renault, L , Molemaker, J., Deutsch, C., and A. Leinweber, 2021b, "Configuration and validation of an oceanic physical and biogeochemical model to investigate coastal eutrophication in the Southern California Bight", *Journal of Advances in Modeling Earth Systems,* vol. *13*, 34 pp., doi.org/10.1029/2020MS002296

Kirk, J. T.O.: 1983, *Light and Photosynthesis in Aquatic Ecosystems*, Cambridge University Press, New York, p. 72.

Lee, Z.-P., K.-P. Du, and R. Arnone (2005), A model for the diffuse attenuation coefficient of downwelling irradiance, *J. Geophys. Res*., 110, C02016, doi:10.1029/2004JC002275.

Mehta, A. J. and E. Partheniades, 1975, "An investigation of the depositional properties of flocculated fine sediment", *Jour. Hyd. Res*, vol 13, n. 4, pp 361 -381.

Mie, Gustav *(1908). "Beiträge zur Optik trüber Medien, speziell kolloidaler Metallösungen". Annalen der Physik.* ***330*** *(3): 377-445.* Bibcode:1908AnP...330..377M. doi:10.1002/andp.19083300302. English translation

Morel, A., and H. Loisel (1998), Apparent optical properties of oceanic water: Dependence on the molecular scattering contribution, *Appl. Opt*., 37, 4765–4776.

Petzold, T. J.: 1972, "Volume Scattering Functions for Selected Ocean Waters", *Scripps Institution of Oceanography, SIO Ref. 72-78*.

Roberts, P.J.W., Snyder, W.H., Baumgartner, D.J., 1989 "Ocean outfalls: I. Submerged waste field formation and II. Spatial evolution of submerged waste field and III. Effect of diffuser design on submerged waste field. J.Hydrol.Eng.115,1–25 26– 48 and 49–70.

Sutula, M., 2019, "Modeling effects of anthropogenic inputs on ocean acidification and hypoxia in the SCB", Validation and Scenarios Subcommittee Meeting Summary, Southern California Coastal Water Research Project, Costa Mesa, September 19, 2019, 8pp.

Uchiyama, Y., Idica, E. Y., McWilliams, J. C., & Stolzenbach, K. D. (2014). Wastewater effluent dispersal in Southern California bays. *Continental Shelf Research*, *76*, 36–52.

APPENDIX A: Examples of Problematic ROMS/BEC Code

roms_08

mod_string_utility.f90 0000644 0001752 0001752
00000004137 12323346012 015364 0
ustar frenzel
cdeutsch
! hf: downloaded Oct 28, 2013 from
! http://coding.derkeiler.com/Archive/Fortran/comp.lang.fortran/2005-03/0762.html
! Original source:
! Figure 3.5B, pg 80, "Upgrading to Fortran 90", by Cooper Redwine,
! 1995 Springer-Verlag, New York.

Page 104:

biology.F 0000644 0001752 0001752
00000037034 12161200113 012660 0 ustar
frenzel cdeutsch
#include "cppdefs.h"
#ifdef BIOLOGY

```
      subroutine biology_tile (istr,iend,jstr,jend)
!
! Compute biological forcing functions as defined by the Fasham et
! al. [JMR, 48, 591-639, 1990].  This routine was originated by John
! Moisan and adpapted for 3D code by MANU Sept. 8 98.   It computes
! r.h.s. terms associated with biological conversions. In this
! particular implementation we have: NO3, NH4, Detritus,
! PHYTOplankton and ZOOplanknton.
!
      implicit none
      integer istr,iend,jstr,jend
#include "param.h"
#include "grid.h"
#include "ocean3d.h"
#include "scalars.h"
      real solar, albedo, trans, PAR0_max, kwater, kphyto, alpha,
     &     K_NO3, K_NH4,  phi,   mu_40,    mu_43,  gmax,   K_Phyt,
     &     beta,  mu_30,  mu_32, mu_50,    mu_52,  mu_53,  pi,
     &           deg2rad,      ccf1,     ccf2,   ccf3,   ccf4
      parameter (
     &   solar   = 1353.,! the solar max is from Brock, 1981
     &   albedo  = 0.04, ! albedo of the ocean surface.
     &   trans   = 0.8,  ! fraction of total radiation
                         ! transmitted through atmosphere
!
```

```
! Potosynthetic Available Radiation (PAR) at the sea surface (without
! correction due to ellipticity of the Earth orbit, absorbtion by the
! effect of solar altitude and atmospheric clouds, see below; 0.43
! here is the estimated PAR fraction of the total solar radiation
!
     &   PAR0_max = solar*trans*0.43*(1.-albedo),
!
! Parameters as in Table 1; Fasham et al. [JMR, 48, 591-639, 1990]
!
     &   kwater = 0.04, ! light attenuation due to sea water [m-1]
     &   kphyto = 0.03, ! light attenuation by Phytoplankton
                        !                    [(m^2 mMol N)-1]
     &   alpha  = 0.025,! initial slope of the P-I curve
                        !                    [(W m-2)-1 d-1]
     &   K_NO3  = 0.5,  ! half-saturation for Phytoplankton NO3
                        !                    uptake [mMol N m-3]
     &   K_NH4  = 0.5,  ! half-saturation for Phytoplankton NH4
                        !                    uptake [mMol N m-3]
     &   phi    = 1.5,  ! Phytoplankton ammonium inhibition
                        !                 parameter [(mMol N)-1]

     &   mu_40  = 0.018,! Phyto loss to sink rate[d-1]
     &   mu_43  = 0.072,! Phyto mortality to Detritus rate d-1]
     &   gmax   = 0.75, ! maximum Zooplankton growth rate [d-1]
     &   beta   = 0.75, ! Zooplankton assimilation efficiency of
                        !                    Zooplankton [n.d.]
     &   K_Phyt = 1.0,  ! Zooplankton half-saturation conts. for
     &                  !                    ingestion [d-1]
     &   mu_50  = 0.025,! Zooplankton loss to sink [d-1]
     &   mu_52  = 0.1,  ! Zooplankton specific excretion rate [d-1]
     &   mu_53  = 0.025,! Zooplankton mortality to Detritus [d-1]

     &   mu_30  = 0.02, ! Detrital loss to sink rate [d-1]
     &   mu_32  = 0.03, ! Detrital breakdown to NH4 rate [d-1]

     &   ccf1   = 0.6071538329,      ! Set OSW Papa CLOUD
     &   ccf2   = 1.187075734,       ! correction coefficients
     &   ccf3   = 0.7726212144,
     &   ccf4   =-0.2782480419,

     &   pi     = 3.14159265358979323846,
     &   deg2rad= 2.*pi/360.)
```

---

page 108-110:

```
! Extract biological variables from tracer arrays; place them into
! scratch variables; restrict their values to be positive definite.
!
        do k=1,N
          NO3_bak(k) =max(t(i,j,k,nnew,iNO3_),0.) ! Nitrate
```

```
          NH4_bak(k) =max(t(i,j,k,nnew,iNH4_),0.) ! Ammonium
          Det_bak(k) =max(t(i,j,k,nnew,iDet_),0.) ! Detritus
          Phyt_bak(k)=max(t(i,j,k,nnew,iPhyt),0.) ! Phytoplankton
          Zoo_bak(k) =max(t(i,j,k,nnew,iZoo_),0.) ! Zooplankton

          NO3(k)  = NO3_bak(k)
          NH4(k)  = NH4_bak(k)
          Det(k)  = Det_bak(k)
          Phyt(k) = Phyt_bak(k)
          Zoo(k)  = Zoo_bak(k)
        enddo
!
! Calulate aJ (here: cos_Znt -- cos of solar zenith angle)
!
        cff=deg2rad*latr(i,j)
        cos_Znt=cos_Thr*cos_dec*cos(cff)+sin_dec*sin(cff)
        if (cos_Znt.gt.0.) then
          PAR0=PAR0_ell*cos_Znt*(1.-ccf1+ccf2*cos_Znt)
     &       *(1.-cloud*( ccf3+ccf4*sqrt(1.-cos_Znt*cos_Znt)))
          do k=1,N                        ! From Eppley, d-1:
            Vp=0.851*1.066**t(i,j,k,nnew,itemp) !   Vp=2.9124317 at
                                          !   t=19.25 degrees
            PARz=PAR0*exp(-abs(z_r(i,j,k))*(kwater+kphyto*Phyt(k)))
            aJ(k)=Vp*alpha*PARz/sqrt(Vp*Vp+alpha*alpha*PARz*PARz)
          enddo
        else
          do k=1,N
            aJ(k)=0.          ! <-- during the night
          enddo
        endif

        DO ITER=1,3   !--> Start internal iterations to achieve
!                       nonlinear backward-implicit solution.
! NO3 uptake by Phyto                                  [1-4]
!
          do k=1,N
            cff=dt_bio*Phyt(k)*aJ(k)*exp(-phi*NH4(k))/(K_NO3+NO3(k))
            NO3(k)=NO3_bak(k)/(1.+cff)
            Phyt(k)=Phyt_bak(k)+cff*NO3(k)
          enddo
!
! NH4 uptake by Phyto                                  [2-4]
!
          do k=1,N
            cff=dt_bio*Phyt(k)*aJ(k)/(K_NH4+NH4(k))
            NH4(k)=NH4_bak(k)/(1.+cff)
            Phyt(k)=Phyt(k)+cff*NH4(k)
          enddo
```

APPENDIX B: CFL Instability Safeguards in Original ROMS-tar Codes by Deutsch and Frenzel

page 1,374

```
!
! After this moment reconstruction is considered complete. The next
! stage is to compute vertical advective fluxes FC. It is expected
! that sinking may occurs relatively fast, the algorithm is designed
! to be free of CFL criterion, which is achieved by allowing
! integration bounds for semi-Lagrangian advective flux to use as
! many grid boxes in upstream direction as necessary.
!
        cff=dt*abs(Wsed(ised))          ! In the two code segments
        do k=1,N                        ! WL is z-coordinate of the
          do i=istr,iend                ! departure point for grid
            FC(i,k-1)=0.                ! box interface z_w with
            WL(i,k)=z_w(i,j,k-1)+cff    ! the same indices;
            WR(i,k)=Hz(i,j,k)*qc(i,k)   ! FC is finite volume flux;
            ksource(i,k)=k              ! ksource(:,k) is index of
          enddo                         ! vertical grid box which
        enddo                           ! contains the departure
        do k=1,N                        ! point (restricted by N);
          do ks=k,N-1                   ! During the search: also
            do i=istr,iend
              if (WL(i,k) .gt. z_w(i,j,ks)) then
                ksource(i,k)=ks+1
                FC(i,k-1)=FC(i,k-1)+WR(i,ks)
              endif
            enddo                       ! add in content of whole
          enddo                         ! grid boxes participating
        enddo       !--> discard WR     ! in FC.

        do k=1,N                        ! Finalize computation of
          do i=istr,iend                ! flux: add fractional part
            ks=ksource(i,k)
            cu=min(1.,(WL(i,k)-z_w(i,j,ks-1))*Hz_inv(i,ks))
            FC(i,k-1)=FC(i,k-1) + Hz(i,j,ks)*cu*( qL(i,ks)
     &                      +cu*( 0.5*(qR(i,ks)-qL(i,ks))
     &           -(1.5-cu)*(qR(i,ks)+qL(i,ks)-2.*qc(i,ks))  ))
          enddo
        enddo             !--> discard WL
        do k=1,N,+1
          do i=istr,iend
            qc(i,k)=qc(i,k) + (FC(i,k)-FC(i,k-1))*Hz_inv(i,k)
          enddo
        enddo    !--> discard everything, except qc,FC(:,0)
!
! Deposition and resuspension near the bottom:  Update thickness of
```

APPENDIX C: CFL Instabilities in Figure 2 of Kessouri et al., (2021b)

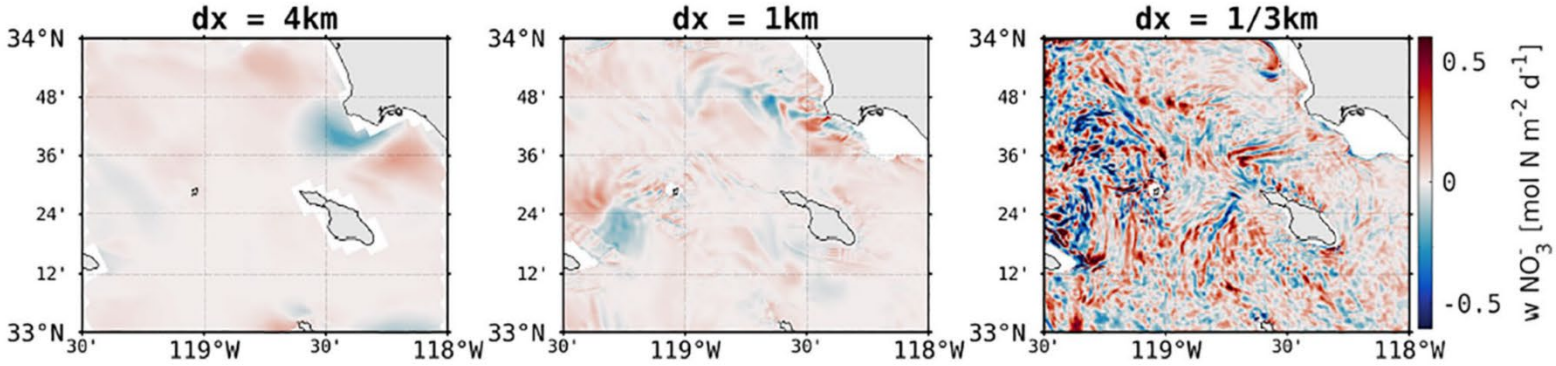

Figure 2. (Upper panel) Time series (1997–2001) of the vertical eddy flux of nitrate at 40-m depth calculated as follows $\overline{wN} = \overline{w}\,\overline{N} + \overline{w'N'}$, where the overbar represents a monthly average, and the prime the deviation from this average, for region covering the entire Southern California Bight (31.4°–35.3°N and 116.5°–121.8°W). The minimum and maximum values (i.e., the envelope) of the flux are shown in blue for the 4-km solution, in red for the 1-km solution, and in green for the 1/3 km. (Lower panel) Snapshot of the vertical flux of nitrate in spring at 40-m off the coast of Palos Verdes that shows higher magnitudes and enhanced variability as resolution increases.